Unraveling the Single-Nanometer Thickness of Shells of Vesicle-Templated Polymer Nanocapsules

Andrew G. Richter,[†] Sergey A. Dergunov,[‡] Mariya D. Kim,[‡] Sergey N. Shmakov,[‡] Sai Venkatesh Pingali,[§] Volker Urban,[§] Yun Liu,[⊥,∥] Eugene Pinkhassik[‡,*]*

[†]Department of Physics and Astronomy, Valparaiso University, Valparaiso, IN 46383, USA; [‡]Department of Chemistry, University of Connecticut, 55 North Eagleville Rd, Storrs, CT 06269-3060, USA, [§]Center for Structural Molecular Biology, Oak Ridge National Laboratory, P.O. Box 2008 MS-6430, Oak Ridge, TN 37831-6430, USA, [⊥]Department of Chemical and Biological Engineering, University of Delaware, Newark, DE 19716, USA, [∥]Center for Neutron Science, National Institute of Standards and Technology, 100 Bureau Dr, Gaithersburg, MD 20899, USA.

Corresponding Authors

*Andrew G. Richter, andy.richter@valpo.edu

*Eugene Pinkhassik, eugene.pinkhassik@uconn.edu.

ABSTRACT Vesicle-templated nanocapsules have emerged as a viable platform for diverse applications. Shell thickness is a critical structural parameter of nanocapsules, where the shell plays a crucial role providing mechanical stability and control of permeability. Here we used small-angle neutron scattering (SANS) to determine the thickness of freestanding and surfactant-stabilized nanocapsules. Despite being at the edge of detectability, we were able to show the polymer shell thickness to be typically 1.0±0.1 nm, which places vesicle-templated nanocapsules among the thinnest materials ever created. The extreme thinness of the shells has implications for several areas: mass-transport through nanopores is relatively unimpeded; pore-forming molecules are not limited to those spanning the entire bilayer; the internal volume of the capsules is maximized; and insight has been gained on how polymerization occurs in the confined geometry of a bilayer scaffold, being predominantly located at the phase-separated layer of monomers and crosslinkers between the surfactant leaflets.

TOC GRAPHICS

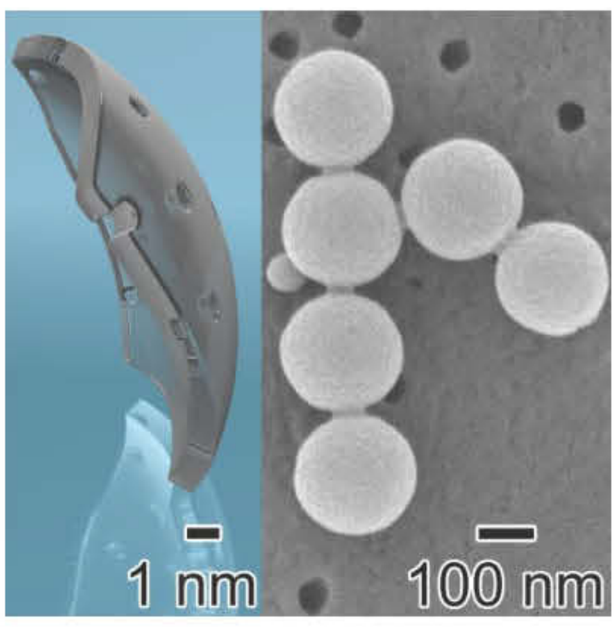

Hollow polymer nanocapsules have emerged as a viable platform for diverse practical applications, including nanoreactors, nanosensors, and containers for the delivery of drugs and

imaging agents.[1-16] In particular, vesicle-templated nanocapsules have garnered special attention in recent years due to the combination of precisely controlled permeability, fast mass transfer, and excellent long-term stability.[2-3, 17] In all of these applications, the shells of the nanocapsules play the crucial role. Vesicle-templated nanocapsules are formed by controlled polymerization and crosslinking of hydrophobic monomers placed in the hydrophobic interior of bilayers of spontaneously formed vesicles. We and others showed successful creation of nanocapsules using vesicles formed from lipids or catanionic (a mixture of cationic and anionic) surfactants.[17-21] Typically, vesicle-templated polymerization produces nanocapsules with a narrow size distribution and an average diameter that can be adjusted in the 50-400 nm range. Size- and charge-selective permeability of the shells is controlled by nanopores with programmed size and chemical environment formed by molecular imprinting using a variety of porogens.[2, 18] Insights into the structural parameters of the shell are critical for understanding the properties of nanocapsule-based devices, including permeability, loading capacity, and mechanical strength. Calculations based on the monomer/scaffold ratio suggested that the polymer shells would have nanometer-scale thicknesses.[18] To date, however, the thickness of freestanding vesicle-templated nanocapsules has not been determined experimentally, due to the difficulty of probing such an extremely thin polymer structure. Lack of this information has limited our abilities in the rational design of bilayer-templated materials. Direct measurement of the thickness of the shells is essential for better understanding of the formation of nanocapsules, investigating structure/property relationships, and development of methods aiming to control the thickness through changes in the formulation of monomer-loaded vesicles.

The kinetics of mass transfer is a critical parameter linked to the thickness of the shells. In previous studies, we observed extremely fast diffusion through the shells of nanocapsules.[3] This property of nanocapsules was essential for enabling fast-acting nanosenors and nanoreactors.[1, 8-9, 15] Generally, the rate of diffusion is inversely proportional to the thickness of a membrane. This consideration assumes similar paths for traversing membranes with different thicknesses. One may imagine, however, that the actual shape of molecular-width channels would likely to be different for 1-nm and 10-nm membranes, resulting in smaller diffusion coefficient for the thicker membranes and further exacerbating the difference in kinetics of mass transfer as a function of the thickness of the shells.

The loading capacity of nanocontainers is another important but frequently overlooked parameter that is highly sensitive to the thickness of the shells. Many applications impose strict limits on the outer size of nanocapsules, making shells thickness especially important. For example, 80-100 nm has been widely recognized as an upper target limit on the size of nanoparticles for desirable mobility characteristics in biomedical applications.[22-24] In this size range, the difference of a few nanometers in shell thickness results in a substantial difference in the inner volume. Figure 1 illustrates the effect of the shell thickness on the ratio between the inner and total volume of nanocapsules.

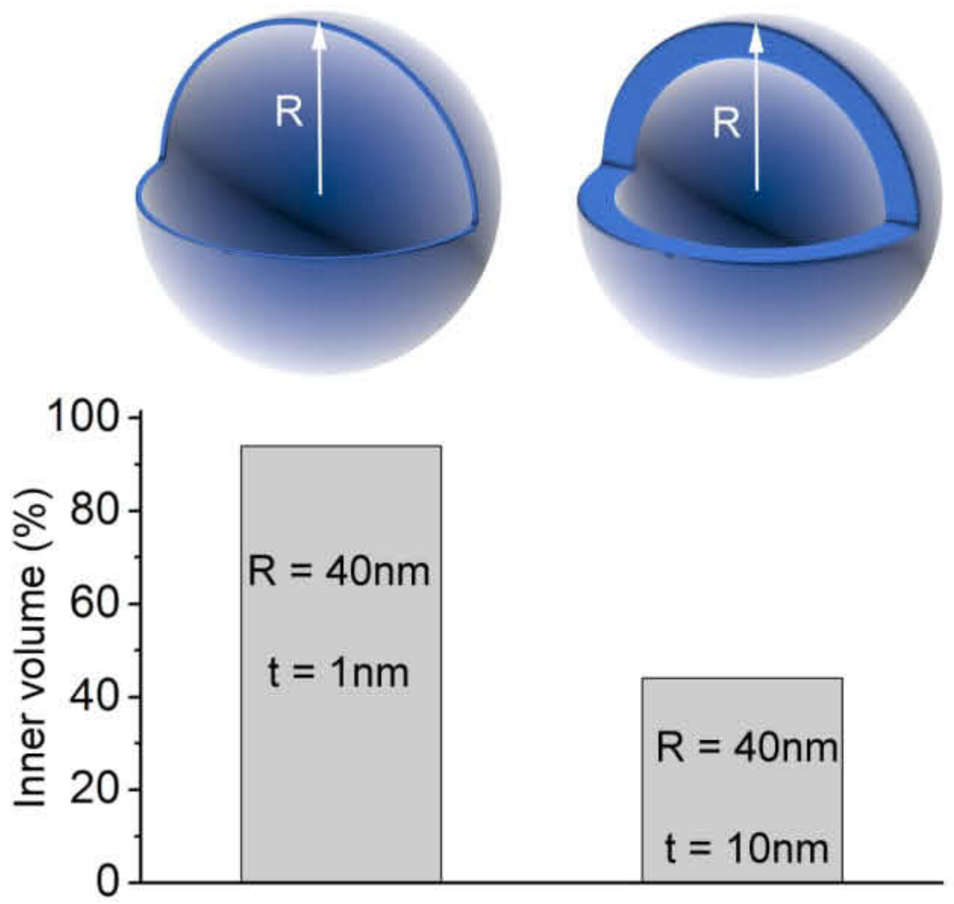

Figure 1. Effect of the wall thickness on the inner volume of nanocapsules. Volumes were calculated for capsules with the outer diameter of 80 nm and shell thickness (t) of 1 nm and 10 nm. Inner volume is shown as the fraction of the total volume of the nanocapsule.

We show the inner volume as a fraction of the total volume for nanocapsules with the diameter of 80 nm, a representative size desirable for biomedical applications, and two shell thicknesses: 1 nm, anticipated for vesicle-templated nanocapsules, and 10 nm, characteristic of nanocapsules produced by other methods, such as layer-by-layer assembly, crosslinking of polymersomes, and emulsion polymerization.[25-27] The results, showing more than 90% of inner volume for 1-nm shells and approx. 40% for 10-nm shells, highlight the sensitivity of the inner volume to the shell thickness and the importance of considering the shell thickness in designing containers with maximized capacity for accommodating molecular cargo.

The ability to gauge the thickness of shells of nanocapsules is essential for evaluating and controlling the most important parameters for practical applications of nanocapsules. The

measurement of the thickness offers insights into the polymerization within the bilayer, establishes the structural parameters of nanocapsules, and offers guidance for the control of pores in the bilayer-templated shells.

The thickness of polymer shells, fabricated using a variety of techniques, has been probed in previous reports using different methods, including transmission electron microscopy and X-ray and neutron scattering.[28-30] As the thickness approaches a single nanometer, it becomes increasingly difficult to obtain an accurate measure. For example, although high-resolution TEM is capable of achieving single-angstrom resolution,[31] accurate measurements of thickness in nanocapsules are hindered by the curvature of the shells. Cryo-TEM also does not offer sufficient resolution for accurate measurement of the vesicle-templated polymer shells thickness, as shown below.

In this work, we use small-angle neutron scattering (SANS) to measure the thickness of freestanding vesicle-templated nanocapsules and to compare the freestanding and surfactant-supported shells. Previously, SANS was used to study hollow shell structures, such as liposomes and surfactant vesicles, polymerized lipid vesicles, vesicles containing monomers or polymerized molecules.[19, 32-37] McKelvey and Kaler used SANS to study surfactant-templated polymer nanocapsules, but only after re-coating the nanocapsules with surfactants to disperse them in water, determining a thickness value for the polymer shell plus the surfactant coating of ~7 nm, acknowledging that they did not have access to the thickness of the polymer shell itself.[32-33]

Polymer nanocapsules used in this study were prepared by the directed assembly method using controlled polymerization of hydrophobic monomers in the interior of bilayers of self-assembled

vesicles (Figure 2).[3, 17, 20] Lipid or surfactant vesicles containing hydrophobic monomers in the bilayer interior were formed by the concurrent loading approach, in which the loading of monomers into the bilayer occurred simultaneously with the formation of the vesicle. The assembly of loaded vesicles was confirmed by DLS, SANS, and SAXS as described previously.[19, 21, 34] Polymerization of monomers followed by removal of the surfactant scaffold produced hollow polymer nanocapsules (Figure 2). A previous study suggested that an inner leaflet could be removed from the nanocapsules by extended washing or alkaline hydrolysis.[17]

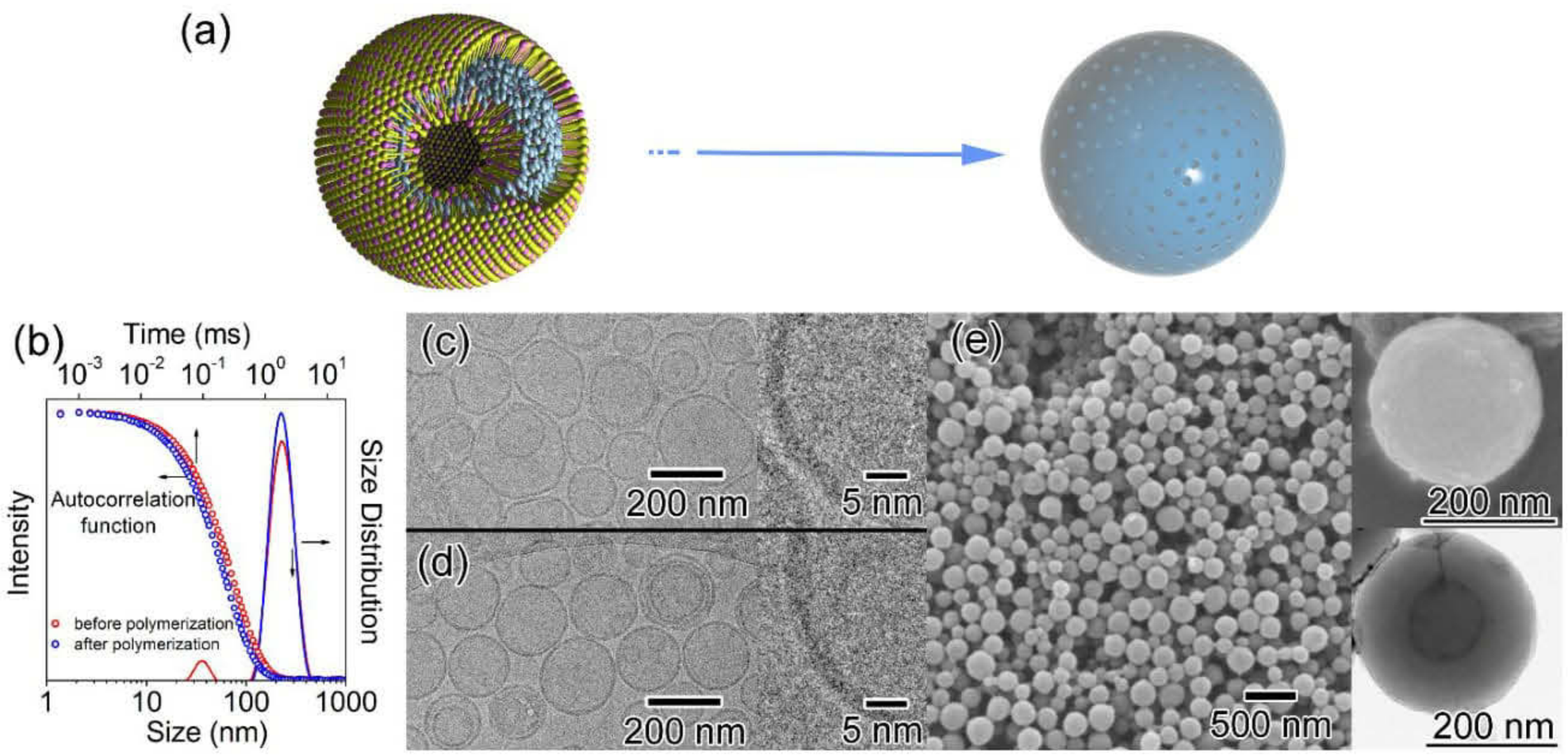

Figure 2. Synthesis and characterization of vesicle-templated nanocapsules. (a) Schematic representation of the preparation of nanocapsules from vesicles: surfactants and monomers are mixed in an aqueous solution producing self-assembled vesicles containing monomers and crosslinkers in the hydrophobic interior of bilayers. Polymerization followed by the removal of the surfactant scaffold yields a suspension of polymer nanocapsules. (b) Typical size distribution (solid line) and autocorrelation function (open circle) of vesicles before and after polymerization determined by dynamic light scattering in aqueous solution. The autocorrelation function

indicates the correlation of scattering intensity at one time with itself at a different time, which is closely related to vesicle size. Typical cryo-TEM images of blank vesicles (c) and vesicles with monomer-loaded bilayers (d). Insets: enlarged cryo-TEM images showing biayers. Typical SEM (e) images of nanocapsules after polymerization and template removal. Insets: SEM and TEM images of freestanding nanocapsules.

Transmission and scanning electron microscopy (TEM and SEM) images showed spherical structures with narrow size distribution (Figure 2) in agreement with previously reported nanocapsules templated by liposomes and surfactant vesicles.[17, 19-20] The average size of nanocapsules isolated after the polymerization of monomers and measured by SEM and TEM (Figure 2e) was identical to the average size of vesicles observed by DLS (Figure 2b). The capsules preserved their spherical shape upon drying (Figure 2e) as expected for highly crosslinked materials. The correlogram in the DLS data (Figure 2b) was indicative of nearly monomodal distribution of vesicles with no evidence of large aggregates. Cryo-TEM data (Figure 2c,d) showed no change in the morphology of vesicles due to loading bilayers with monomers and highlighted the difficulty with accurate measurement of the shell thickness with electron microscopy.

SANS measurements were performed with the CG-3 Bio-SANS instrument at the High Flux Isotope Reactor (HFIR) facility of Oak Ridge National Laboratory and at the NC-7 SANS instrument at the National Institute of Standards and Technology's Center for Neutron Research (NCNR).[38-39] Quartz cells of 1 or 2 mm thickness were used to hold the liquid samples. At both

facilities, we collected data with $\lambda = 6\,\text{Å}$ $(\Delta\lambda/\lambda \approx 12\%)$ at 2 different detector-distance configurations, giving a Q-range, where $Q = (4\pi/\lambda)\sin\theta$ and θ is the scattering angle, of ~0.01 Å^{-1} to ~0.5 Å^{-1}. Both beamlines use Ordela area detectors. The scattering curves, $I(Q)$ versus Q, were obtained by azimuthally averaging the processed 2D images, which were normalized to incident beam monitor counts, and corrected for detector dark current, pixel sensitivity and empty beam scattering background.[40] In order to maximize contrast, fully hydrogenated monomers were used to form the nanocapsules which were dispersed in deuterated benzene or D_2O.

Solvent background subtraction is performed by scaling a solvent-only scan and subtracting it from the sample scan such that at the highest Q values, where incoherent scattering is dominant, the result of the subtraction is on the order of 10^{-3} to 10^{-4} cm^{-1}. At the highest Q values, the scattering should go as Q^{-4} (Porod scattering),

$$I(Q) = 2\pi\Delta\rho^2 \frac{S}{V}\frac{1}{Q^4} + B$$

where $\Delta\rho$ is the scattering length density contrast of the shell and solvent, $\frac{S}{V}$ is the surface to volume ration, and B is the background. We check the background subtraction by plotting IQ^4 vs Q^4, which results in a zero slope if all the background has been removed.

SANS curves of geometric objects display one or two Guinier regions, places where the power law behavior of the scattering changes. For hollow vesicles, there are two: one at low Q going from Q^0 to Q^{-2} due to the radius of the sphere; and one at higher Q going from Q^{-2} to Q^{-4} due to

the thickness of the shell.[41] For large vesicles, the radius Guinier region is typically below the minimum Q range of the SANS instrument. Therefore, our focus is on observing a power law region with Q^{-2} and analyzing where it curves over to Q^{-4}. Note that an exponent somewhat deviating from -2 can be observed for vesicles due to roughness of the surface, porosity of the shell, or the influence of scattering from other length-scales or objects in the sample.

Due to the presence of unknown particulates in our polymerized samples, we are unable to use simple form functions to fit the curves and determine the thickness of the shells. Instead, our main method of analysis is to use a modified Guinier analysis for thin sheets. In the thickness Guinier region the approximate form for the SANS curve is

$$I(Q) = \frac{A}{Q^2} e^{-Q^2 {R_t}^2}$$

where A is a constant related to the scattering contrast, and R_t is the thickness radius of gyration, which is related to the thickness of the shell as

$$R_t = \frac{1}{\sqrt{12}} T .$$

Therefore, a plot of $\ln(IQ^2)$ vs Q^2, called a modified Guinier plot, should yield a straight line with slope $-R_t^2$ in the Guinier region.[42] This approximation only rigorously holds for $Q_{\max} R_t = 1$, where $Q_{\max}$ is the highest Q value used in the linear fit, though in practice the

Guinier region is often located where $QR_t \approx 0.1-0.9$, so it is common to just restrict $Q_{\max}R_t < 0.9$. We have also used Guinier-Porod modeling to check the Guinier results for samples that have significant noise or limited linear ranges in the modified Guinier plots (see supporting information).[43]

Figure 3A shows the SANS curve for a sample consisting of 220 nm nanocapsules dispersed in d-benzene. As expected for a shell structure, a Q^{-2} region exists, followed by a Q^{-4} region. There is also a lower Q feature that may be due to particulates, perhaps collapsed polymer shells or polymer spheres that formed in surfactant micelles. It is also possible that it corresponds to a length-scale representative of the polymer network in the shell; future work may explore that possibility. From other experiments in which we varied the deuterium content of the monomers (not shown), we have observed that this feature is correlated to the polymer material itself. In this paper, we are concerned with curve over to Q^{-4} scattering, since that is correlated to the shell thickness.

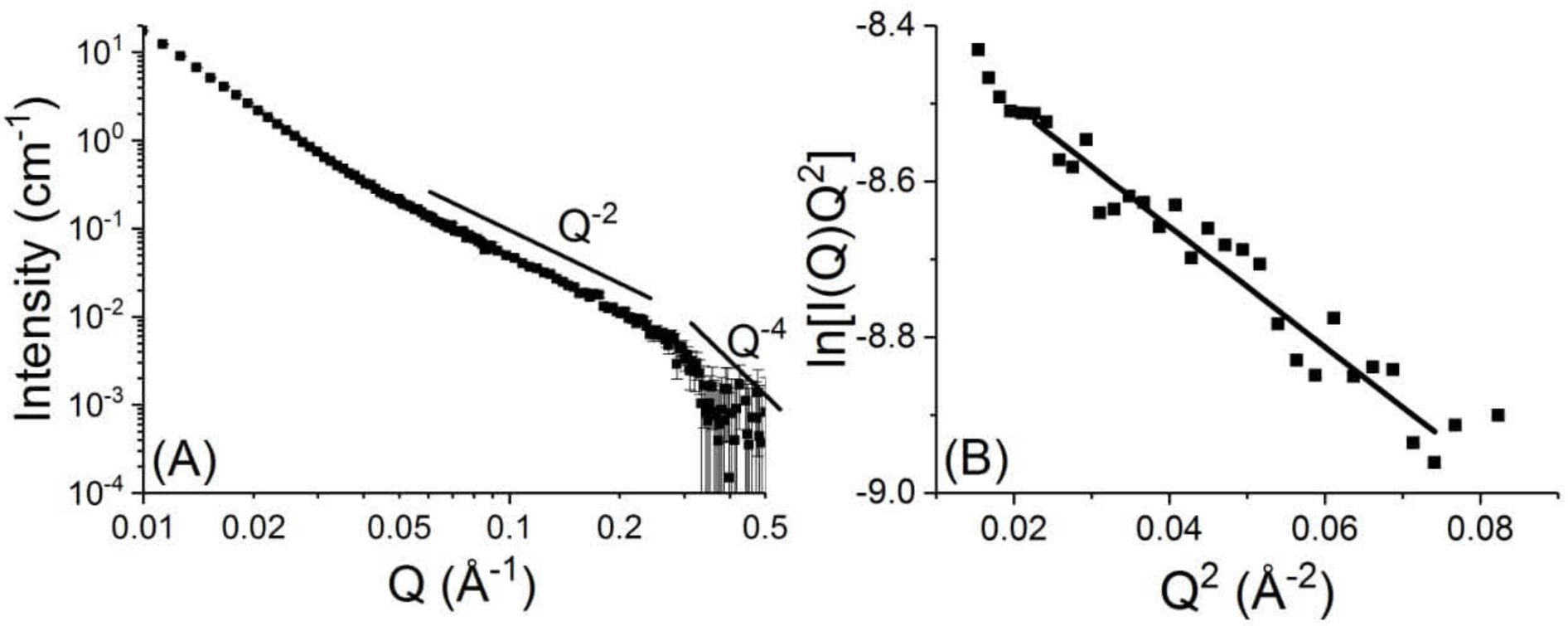

Figure 3. (A) SANS curve for nanocapsules dispersed in d-benzene after solvent background subtraction. The lines show the Q^{-2} and Q^{-4} regions for a shell structure. Because the shell is so thin, the Guinier region is near the maximum Q value obtainable at the SANS instruments and the intensity is very low. (B) A modified Guinier plot and fit for nanocapsules dispersed in d-benzene (from a different sample than shown in panel A, with better statistics). From the slope of the linear fit (solid line), a shell thickness of 10.0 ± 0.3 Å was determined. Error bars are not shown for clarity; they are similar to the size of the scatter in the data.

Because the polymer shells are so thin, the Q^{-2} scattering does not terminate until at high Q values, near the limit for the instruments. In addition, because the intensity decreases as Q^{-2} over this large range, by the time the thickness Guinier is reached, the intensity is just above the incoherent background, making statistically significant data collection difficult and the data noisy. Samples generally dispersed well in benzene, but we did notice aggregation or precipitation for some samples, limiting our ability to scan for arbitrarily long times. Therefore, we integrated over times ranging from 15 minutes up to 4 hours to improve the statistics, while avoiding complications due to precipitation. Figure 3B shows a modified Guinier plot for a well-dispersed sample that was scanned for 4 hours.

For the sample shown in Fig. 3B, the slope indicates the thickness is 10.0 ± 0.3 Å, which matches well with our expectations and indicates an extremely thin shell. This error was determined by the fit, but underestimates the actual uncertainty due to the fact that different starting and ending data points can be reasonably selected. In order to assess that error, we chose

a range of starting and ending points, performed fits, and then found the midpoint and range of those values. For this sample, that analysis yielded a thickness of 10.0 Å with an estimated uncertainty of 0.9 Å. An additional source of error comes from the uncertainty in the scaling factor for the background subtraction. More aggressive background subtraction results in a steeper slope and larger thickness. Because we checked the background subtraction using a Porod plot, our scaling factor is tightly constrained, but uncertainty in that value increases the uncertainty in the thickness determination. Therefore, we estimate the uncertainty to be closer to 1.0 Å and report the shell thickness for this sample as 10.0 ± 1.0 Å. In total, the five samples we examined showed thicknesses close to this value, ranging from 9.6 Å to 11.4 Å. The above uncertainty estimation methodology was validated by generating Guinier-Porod modeled intensity curves, offsetting the shell thickness by ± 1.0 Å, and evaluating the reduced χ^2, noting that it increased by more than 40% (see supporting information).

These results build upon our previous study of the distribution of monomers within the bilayer.[19, 21, 34] We found that the bilayers of phospholipid vesicles swell by about 4 Å when saturated with monomers due to phase separation of the monomers between the bilayer leaves. By knowing the molar ratio of monomers to lipids and the surface area of the lipids, we were able to determine that this accounted for only roughly half of the monomers, meaning that the rest were distributed within the hydrophobic tails of the lipids.[34, 44] During polymerization, we expected the concentrated monomers to readily cross-link, forming the shell, but how the diffusely distributed monomers would contribute to the shell was less clear. The thickness of the hydrophobic interior is approx. 3 nm; therefore, we hypothesized that either monomers would

migrate towards the developing polymer shell, creating a ~1 nm thick, relatively dense shell; or they would polymerize into a more sponge-like, ~3 nm thick shell. The data produced in this study indicated that the monomers in the scaffold do migrate towards the phase separated monomers between the bilayer leaves during polymerization, forming an extremely thin, relatively dense, shell.

Newly gained understanding of the formation of the shells offers further insights into the role of porogens in templating nanopores in the shells. Since the polymerization appears to occur predominantly in the interstitial phase-separated layer, localization of porogens in the interstitial layer would result in effective formation of pores without the need for porogens to span the bilayer. Multiple studies suggested that large hydrophobic molecules tend to partition deep inside the bilayer,[45-47] supporting the notion that a broad variety of hydrophobic molecules could serve as porogens and expanding the scope of the imprinting method for the formation of nanopores in the shells.

Due to the templating process used, our nanocapsules are hydrophobic. Many applications, however, require dispersing the nanocapsules in water. One way to accomplish this is to use surfactants to stabilize aqueous dispersions, e.g., when hydrating dried nanocapsules. The surfactants will preferentially coat the nanocapsules surfaces to reduce the energy of the boundary. Figure 4 shows the effect of the surfactant on the thickness feature at high Q. Here, SANS curves were obtained for nanocapsules from the same batch that was split into to parts for different processing. One fraction was washed extensively, freeze-dried, and dispersed in d-benzene. Another fraction was stabilized with a solution of Triton X-100 in D_2O and washed with D_2O until no surfactant micelles remained in solution as evidenced by DLS and SANS data.

In d-benzene, the thickness Guinier feature is located around 0.3 $Å^{-1}$ whereas in D_2O, the feature moves to lower Q, around 0.1 $Å^{-1}$, suggesting that the thickness is roughly three times larger. From modified Guinier analysis, without surfactants this sample has a shell thickness of 11.4 ± 0.7 Å. Addition of surfactants increased the measured thickness to 31.3 ± 1.7 Å, indicating that the surfactants add a combined total of nearly 20 Å on the inner and outer sides of the shell wall. These measurements are comparable with the thickness of monomer-loaded bilayers obtained from cryo-TEM (Figure 2d). Another sample studied in this same manner showed the same results. These findings correlate well with the literature data on the adsorption of surfactants on hydrophobic surfaces.[48-51] Aqueous dispersions of nanocapsules investigated here were stabilized by Triton X-100 without removal of the inner surfactant layer. Under these conditions, one may expect a single layer of Triton X-100 outside and a single layer of residual SDBS/CTAT mixture on the inside of the shell. The total increase in thickness surfactant layer is consistent with literature data on the formation of a single layer of each respective surfactant adsorbing on the surface by its hydrophobic tail.[52-53]

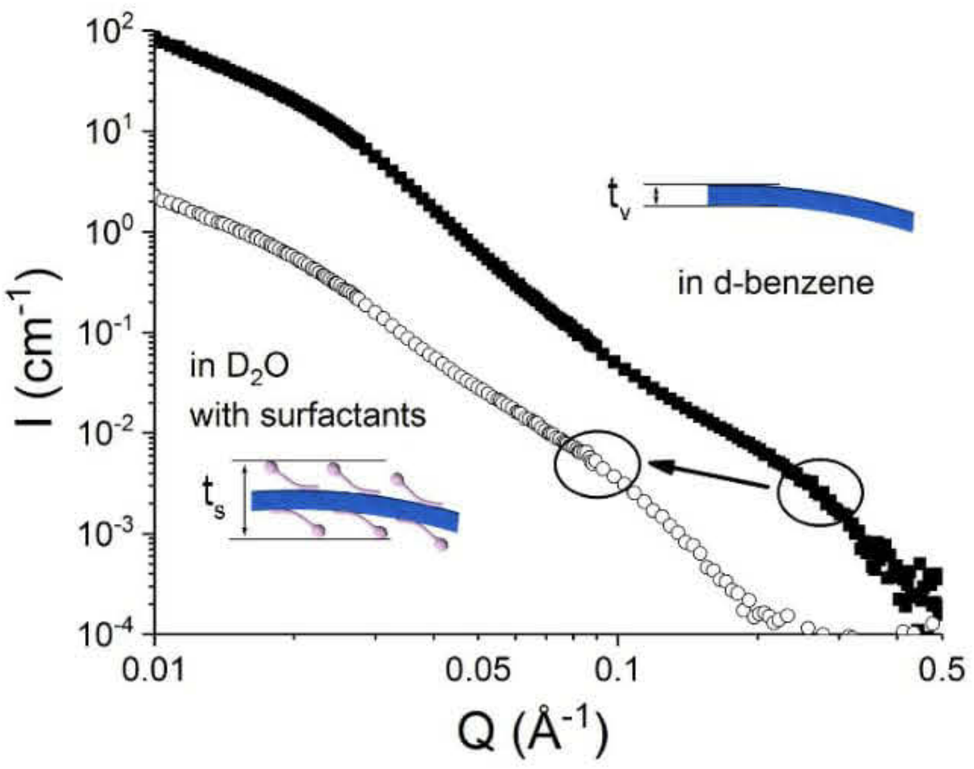

Figure 4. Comparison of the SANS curves for nanocapsules dispersed in d-benzene (black squares) and the same batch of nanocapsules stabilized with surfactants and dispersed in D_2O (open circles; divided by 10 for clarity). The thickness Guinier region is circled for both curves. It moves from near 0.3 $Å^{-1}$ to near 0.1 $Å^{-1}$, indicating that the thickness roughly triples due to the surfactant coating on both sides of the shell wall.

In conclusion, we have measured the thickness of freestanding polymer vesicle-templated nanocapsules using SANS and confirmed the single-nanometer thickness of the shells, showing that the shells of these nanocapsules are among the thinnest materials with readily tunable permeability. Based on this new structural information, it appears that polymerization within the bilayer template is centered on the phase-separated interstitial layer that attracts other monomers dispersed within the bilayer to form a densely packed crosslinked shell. We have also explained how pores can be imprinted in the bilayer-templated materials without the need for membrane-spanning templates, greatly widening the variety of porogens that can be employed.

ASSOCIATED CONTENT

Supporting Information

The following file is available free of charge.

Full experimental detail on the synthesis and characterization of vesicle-templated polymer nanocapsules and details on the analysis of SANS data (PDF)

AUTHOR INFORMATION

Corresponding Author

*Phone: (1) 860-486-3214. Fax: (1) 860-486-2981. Emails: andy.richter@valpo.edu

eugene.pinkhassik@uconn.edu

Notes

The authors declare no competing financial interests.

ACKNOWLEDGMENTS

This work was supported by the National Science Foundation (CHE-1709921, CHE-1522525, CHE-1316680, and CHE-1012951). SEM and TEM studies were performed using the facilities in the UConn/FEI Center for Advanced Microscopy and Materials Analysis (CAMMA). Neutron scattering research conducted at the Bio-SANS instrument, a DOE Office of Science, Office of Biological and Environmental Research resource, used resources at the High Flux Isotope Reactor, a DOE Office of Science, Scientific User Facility operated by the Oak Ridge National Laboratory. We acknowledge the support of the National Institute of Standards and Technology, U.S. Department of Commerce, in providing the neutron research facilities used in this work. Certain commercial equipment, instruments, or materials are identified in this paper to foster understanding. Such identification does not imply recommendation or endorsement by the National Institute of Standards and Technology, nor does it imply that the materials or equipment identified are necessarily the best available for the purpose.

REFERENCES

(1) Dergunov, S. A.; Khabiyev, A. T.; Shmakov, S. N.; Kim, M. D.; Ehterami, N.; Weiss, M. C.; Birman, V. B.; Pinkhassik, E. Encapsulation of Homogeneous Catalysts in Porous Polymer Nanocapsules Produces Fast-Acting Selective Nanoreactors. *ACS Nano* **2016,** *10*, 11397-11406.

(2) Dergunov, S. A.; Durbin, J.; Pattanaik, S.; Pinkhassik, E. pH-Mediated Catch and Release of Charged Molecules with Porous Hollow Nanocapsules. *J. Am. Chem. Soc.* **2014,** *136*, 2212-5.

(3) Dergunov, S. A.; Miksa, B.; Ganus, B.; Lindner, E.; Pinkhassik, E. Nanocapsules With ''Invisible'' Walls. *Chem. Commun.* **2010,** *46*, 1485-1487.

(4) Dergunov, S. A.; Pinkhassik, E. Synergistic Co-Entrapment and Triggered Release in Hollow Nanocapsules with Uniform Nanopores. *J. Am. Chem. Soc.* **2011,** *133*, 19656-19659.

(5) Dergunov, S. A.; Pinkhassik, E. Hollow Nanocapsules in Biomedical Imaging Applications. In *Nanotechnology for Biomedical Imaging and Diagnostics*; Berezin, M.Y., Ed.; Wiley: Hoboken, 2014; pp 83-109.

(6) Ehterami, N.; Dergunov, S. A.; Ussipbekova, Y.; Birman, V. B.; Pinkhassik, E. Catalytic Ship-in-a-Bottle Assembly Within Hollow Porous Nanocapusles. *New J. Chem.* **2014,** *38*, 481-485.

(7) Gustafson, T. P.; Dergunov, S. A.; Akers, W. J.; Cao, Q.; Magalotti, S.; Achilefu, S.; Pinkhassik, E.; Berezin, M. Y. Blood Triggered Rapid Release Porous Nanocapsules. *RSC Advances* **2013,** *3*, 5547-5555.

(8) Kim, M. D.; Dergunov, S. A.; Lindner, E.; Pinkhassik, E. Dye-Loaded Porous Nanocapsules Immobilized in a Permeable Polyvinyl Alcohol Matrix: A Versatile Optical Sensor Platform. *Anal. Chem.* **2012,** *84*, 2695-2701.

(9) Zhegalova, N. G.; Dergunov, S. A.; Wang, S. T.; Pinkhassik, E.; Berezin, M. Y. Design of Fluorescent Nanocapsules as Ratiometric Nanothermometers. *Chem. Eur. J.* **2014,** *20*, 10292-10297.

(10) Sun, H.; Chen, C.-K.; Cui, H.; Cheng, C. Crosslinked Polymer Nanocapsules. *Polym. Int.* **2016,** *65*, 351-361.

(11) Musyanovych, A.; Landfester, K. Polymer Micro- and Nanocapsules as Biological Carriers with Multifunctional Properties. *Macromol. Biosci.* **2014,** *14*, 458-477.

(12) Timin, A. S.; Gould, D. J.; Sukhorukov, G. B. Multi-Layer Microcapsules: Fresh Insights and New Applications. *Expert Opin. Drug Deliv.* **2017,** *14*, 583-587.

(13) Xiao-ying, Z.; Pei-ying, Z. Polymersomes in Nanomedicine - A Review. *Current Nanoscience* **2017,** *13*, 124-129.

(14) Jia, Y.; Shmakov, S. N.; Register, P.; Pinkhassik, E. Size-Selective Yolk-Shell Nanoreactors with Nanometer-Thin Porous Polymer Shells. *Chem. Eur. J.* **2015,** *21*, 12709-12714.

(15) Maclin, A. Q.; Kim, M. D.; Dergunov, S. A.; Pinkhassik, E.; Lindner, E. Small-Volume pH Sensing with a Capillary Optode Utilizing Dye-Loaded Porous Nanocapsules in a Hydrogel Matrix. *Electroanalysis* **2015,** *27*, 733-744.

(16) Jia, Y.; Shmakov, S. N.; Pinkhassik, E. Controlled Permeability in Porous Polymer Nanocapsules Enabling Size- and Charge-Selective SERS Nanoprobes. *ACS Appl. Mater. Interfaces* **2016,** *8*, 19755-19763.

(17) Dergunov, S. A.; Kesterson, K.; Li, W.; Wang, Z.; Pinkhassik, E. Synthesis, Characterization, and Long-Term Stability of Hollow Polymer Nanocapsules with Nanometer-Thin Walls. *Macromolecules* **2010,** *43*, 7785-7792.

(18) Dergunov, S. A.; Pinkhassik, E. Functionalization of Imprinted Nanopores in Nanometer-Thin Organic Materials. *Angew. Chem. Int. Ed.* **2008,** *47*, 8264-8267.

(19) Dergunov, S. A.; Richter, A. G.; Kim, M. D.; Pingali, S. V.; Urban, V. S.; Pinkhassik, E. Synergistic Self-Assembly of Scaffolds and Building Blocks for Directed Synthesis of Organic Nanomaterials. *Chem. Commun.* **2013,** *49*, 11026-11028.

(20) Kim, M. D.; Dergunov, S. A.; Pinkhassik, E. Directed Assembly of Vesicle-Templated Polymer Nanocapsules under Near-Physiological Conditions. *Langmuir* **2015,** *31*, 2561-2568.

(21) Kim, M. D.; Dergunov, S. A.; Richter, A. G.; Durbin, J.; Shmakov, S. N.; Jia, Y.; Kenbeilova, S.; Orazbekuly, Y.; Kengpeiil, A.; Lindner, E.; Pingali, S. V.; Urban, V. S.; Weigand, S.; Pinkhassik, E. Facile Directed Assembly of Hollow Polymer Nanocapsules within Spontaneously Formed Catanionic Surfactant Vesicles. *Langmuir* **2014,** *30*, 7061-7069.

(22) Tang, L.; Yang, X.; Yin, Q.; Cai, K.; Wang, H.; Chaudhury, I.; Yao, C.; Zhou, Q.; Kwon, M.; Hartman, J. A.; Dobrucki, I. T.; Dobrucki, L. W.; Borst, L. B.; Lezmi, S.; Helferich, W. G.; Ferguson, A. L.; Fan, T. M.; Cheng, J. Investigating the Optimal Size of Anticancer Nanomedicine. *Proc. Natl. Acad. Sci. U.S.A.* **2014,** *111*, 15344-15349.

(23) Shah, R. R.; O'Hagan, D. T.; Amiji, M. M.; Brito, L. A. The Impact of Size on Particulate Vaccine Adjuvants. *Nanomedicine* **2014,** *9*, 2671-2681.

(24) Banik, B. L.; Fattahi, P.; Brown, J. L. Polymeric Nanoparticles: The Future of Nanomedicine. *Wiley Interdiscip. Rev. Nanomed. Nanobiotechnol.* **2016,** *8*, 271-299.

(25) Rivera, M. C.; Pinheiro, A. C.; Bourbon, A. I.; Cerqueira, M. A.; Vicente, A. A. Hollow Chitosan/Alginate Nanocapsules for Bioactive Compound Delivery. *Int. J. Biol. Macromol.* **2015,** *79*, 95-102.

(26) Romio, A. P.; Sayer, C.; Araújo, P. H. H.; Al-Haydari, M.; Wu, L.; da Rocha, S. R. P. Nanocapsules by Miniemulsion Polymerization with Biodegradable Surfactant and Hydrophobe. *Macromol. Chem. Phys.* **2009,** *210*, 747-751.

(27) Discher, D. E.; Ahmed, F. Polymersomes. *Annu. Rev. Biomed. Eng.* **2006,** *8*, 323-341.

(28) Rübe, A.; Hause, G.; Mäder, K.; Kohlbrecher, J. Core-Shell Structure of Miglyol/Poly(d,l-Lactide)/Poloxamer Nanocapsules Studied by Small-Angle Neutron Scattering. *J. Control. Release* **2005,** *107*, 244-252.

(29) Choi, I.; Malak, S. T.; Xu, W.; Heller, W. T.; Tsitsilianis, C.; Tsukruk, V. V. Multicompartmental Microcapsules from Star Copolymer Micelles. *Macromolecules* **2013,** *46*, 1425-1436.

(30) Choi, S. H.; Lee, J.-H.; Choi, S.-M.; Park, T. G. Thermally Reversible Pluronic/Heparin Nanocapsules Exhibiting 1000-Fold Volume Transition. *Langmuir* **2006,** *22*, 1758-1762.

(31) Williams, D. B.; Carter, C. B. *Transmission Electron Microscopy. A Textbook for Materials Science*. Springer: New York, 2009.

(32) McKelvey, C. A.; Kaler, E. W. Characterization of Nanostructured Hollow Polymer Spheres with Small-Angle Neutron Scattering (SANS). *J. Colloid. Interf. Sci.* **2002,** *245*, 68-74.

(33) McKelvey, C. A.; Kaler, E. W.; Zasadzinski, J. A.; Coldren, B.; Jung, H. T. Templating Hollow Polymeric Spheres from Catanionic Equilibrium Vesicles: Synthesis and Characterization. *Langmuir* **2000,** *16*, 8285 – 8290.

(34) Richter, A. G.; Dergunov, S. A.; Ganus, B.; Thomas, Z.; Pingali, S. V.; Urban, V.; Liu, Y.; Porcar, L.; Pinkhassik, E. Scattering Studies of Hydrophobic Monomers in Liposomal Bilayers: An Expanding Shell Model of Monomer Distribution. *Langmuir* **2011,** *27*, 3792-3797.

(35) Chécot, F.; Rodríguez-Hernández, J.; Gnanou, Y.; Lecommandoux, S. pH-Responsive Micelles and Vesicles Nanocapsules Based on Polypeptide Diblock Copolymers. *Biomol. Eng.* **2007,** *24*, 81-85.

(36) Dubbert, J.; Honold, T.; Pedersen, J. S.; Radulescu, A.; Drechsler, M.; Karg, M.; Richtering, W. How Hollow Are Thermoresponsive Hollow Nanogels? *Macromolecules* **2014,** *47*, 8700-8708.

(37) Egelhaaf, S. U.; Schurtenberger, P. Micelle-to-Vesicle Transition: A Time-Resolved Structural Study. *Phys. Rev. Lett.* **1999,** *82*, 2804-2807.

(38) Lynn, G. W.; Heller, W.; Urban, V.; Wignall, G. D.; Weiss, K.; Myles, D. A. A. Bio-SANS —A Dedicated Facility for Neutron Structural Biology at Oak Ridge National Laboratory. *Physica B: Condensed Matter* **2006,** *385–386,* 880-882.

(39) Glinka, C. J.; Barker, J. G.; Hammouda, B.; Krueger, S.; Moyer, J. J.; Orts, W. J. The 30 m Small-Angle Neutron Scattering Instruments at the National Institute of Standards and Technology. *J. Appl. Crystallogr.* **1998,** *31*, 430-445.

(40) Kline, S. Reduction and Analysis of SANS and USANS Data Using IGOR Pro. *J. Appl. Crystallogr.* **2006,** *39*, 895-900.

(41) Glatter, O.; Kratky, O. *Small Angle X-ray Scattering*. Academic Press: New York, 1982.

(42) Brasher, L. L.; Kaler, E. W. A Small-Angle Neutron Scattering (SANS) Contrast Variation Investigation of Aggregate Composition in Catanionic Surfactant Mixtures. *Langmuir* **1996,** *12*, 6270-6276.

(43) Hammouda, B. A New Guinier–Porod Model. *J. Appl. Crystallogr.* **2010,** *43*, 716-719.

(44) Dergunov, S. A.; Schaub, S. C.; Richter, A.; Pinkhassik, E. Time-Resolved Loading of Monomers into Bilayers with Different Curvature. *Langmuir* **2009,** *26*, 6276-6280.

(45) Santos, S. M.; Dinis, A. M.; Peixoto, F.; Ferreira, L.; Jurado, A. S.; Videira, R. A. Interaction of Fullerene Nanoparticles With Biomembranes: From the Partition in Lipid Membranes to Effects on Mitochondrial Bioenergetics. *Toxicol. Sci.* **2014,** *138*, 117-129.

(46) Chen, Y.; Bose, A.; Bothun, G. D. Controlled Release from Bilayer-Decorated Magnetoliposomes via Electromagnetic Heating. *ACS Nano* **2010,** *4*, 3215-3221.

(47) Li, Y.; Gu, N. Computer Simulation of the Inclusion of Hydrophobic Nanoparticles into a Lipid Bilayer. *J. Nanosci. Nanotechnol.* **2010,** *10*, 7616-7619.

(48) Despert, G.; Oberdisse, J. Formation of Micelle-Decorated Colloidal Silica by Adsorption of Nonionic Surfactant. *Langmuir* **2003,** *19*, 7604-7610.

(49) Edwards, D. A.; Adeel, Z.; Luthy, R. G. Distribution of Nonionic Surfactant and Phenanthrene in a Sediment/Aqueous System. *Environ. Sci. Technol.* **1994,** *28*, 1550-1560.

(50) Thakkar, K.; Patel, V.; Ray, D.; Pal, H.; Aswal, V. K.; Bahadur, P. Interaction of Imidazolium Based Ionic Liquids with Triton X-100 Micelles: Investigating the Role of the Counter Ion and Chain Length. *RSC Advances* **2016,** *6*, 36314-36326.

(51) Goyal, P. S.; Menon, S. V. G.; Dasannacharya, B. A.; Thiyagarajan, P. SANS Study of Micellar Structure and Interactions in Triton X-100 Solutions. *Physica B: Condensed Matter* **1995,** *213*, 610-612.

(52) Tang, B.; Pal, P.; Gosalvez, M. A.; Shikida, M.; Sato, K.; Amakawa, H.; Itoh, S. Ellipsometry Study of the Adsorbed Surfactant Thickness on Si{1 1 0} and Si{1 0 0} and the Effect of Pre-Adsorbed Surfactant Layer on Etching Characteristics in TMAH. *Sensor. Actuat. A: Phys* **2009,** *156*, 334-341.

(53) Tummala, N. R.; Morrow, B. H.; Resasco, D. E.; Striolo, A. Stabilization of Aqueous Carbon Nanotube Dispersions Using Surfactants: Insights from Molecular Dynamics Simulations. *ACS Nano* **2010,** *4*, 7193-7204.